Chemical Senses, 2023, **48**, 1–8
https://doi.org/10.1093/chemse/bjad003
Advance access publication 6 February 2023
Original Article

Original Article

Paradoxical electro-olfactogram responses in TMEM16B knock-out mice

Giorgia Guarneri[1], Simone Pifferi[2], Michele Dibattista[3], Johannes Reisert[4] and Anna Menini[1]

[1]Neuroscience Area, SISSA, Scuola Internazionale Superiore di Studi Avanzati, Trieste, Italy
[2]Department of Experimental and Clinical Medicine, Università Politecnica delle Marche, Ancona, Italy
[3]Department of Translational Biomedicine and Neuroscience, University of Bari Aldo Moro, Bari, Italy
[4]Monell Chemical Senses Center, Philadelphia, USA

Corresponding author: Michele Dibattista, Department of Translational Biomedicine and Neuroscience, University of Bari Aldo Moro, Piazza Giulio Cesare 11, Bari, Italy. Email: michele.dibattista@uniba.it; Johannes Reisert: Monell Chemical Senses Center, 3500 Market Street, Philadelphia, PA. Tel: 267 519 4795; Email: jreisert@monell.org; Anna Menini, SISSA, Neuroscience Area, Via Bonomea 265, Trieste, Italy. Tel: +39 0403787706. Email: anna.menini@sissa.it

Abstract

The Ca^{2+}-activated Cl^- channel TMEM16B carries up to 90% of the transduction current evoked by odorant stimulation in olfactory sensory neurons and control the number of action potential firing and therefore the length of the train of action potentials. A loss of function approach revealed that TMEM16B is required for olfactory-driven behaviors such as tracking unfamiliar odors. Here, we used the electro-olfactogram (EOG) technique to investigate the contribution of TMEM16B to odorant transduction in the whole olfactory epithelium. Surprisingly, we found that EOG responses from *Tmem16b* knock out mice have a bigger amplitude compared to those of wild type. Moreover, the kinetics of EOG responses is faster in absence of TMEM16B, while the ability to adapt to repeated stimulation is altered in knock out mice. The larger EOG responses in *Tmem16b* knock out may be the results of the removal of the clamping and/or shunting action of the Ca^{2+}-activated Cl^- currents leading to the paradox of having smaller transduction current but larger generator potential.

Keywords: Ca^{2+}-activated Cl^- currents, ANO2, olfactory sensory neurons, olfactory transduction

Introduction

In physiology, sensory transduction is the transformation of a sensory stimulus into neuronal activity and involves a variety of different mechanisms. In olfaction, this is the transformation of chemical signals (odorants) into an electric one that is then transmitted to the brain (Genovese et al., 2021; Kleene, 2008; Pifferi et al., 2012; Tirindelli et al., 2009; Torre et al., 1995).

In olfactory sensory neurons (OSNs), odorant transduction is triggered by the binding of odorant molecules to odorant receptors (ORs) located in the ciliary membrane of the cell (Mombaerts, 2004). The conformational change of the OR leads to an increase in intraciliary cAMP, which in turn favors the opening of cyclic nucleotide-gated (CNG) channels (Bradley et al., 2005; Brunet et al., 1996; Nakamura and Gold, 1987). Na^+ and Ca^{2+} influx now increases, thus generating a receptor current. Then, the receptor current is further amplified by the efflux of Cl^- via the opening of TMEM16B (also called Anoctamin 2), a Ca^{2+}-activated Cl^- channel (Boccaccio et al., 2021; Dibattista et al., 2017; Neureither et al., 2017; Stephan et al., 2009). Interestingly, OSNs are one of the rare cases in which a Cl^- current is depolarizing due to a quite positive equilibrium potential for Cl^- (Kaneko et al., 2004; Reuter et al., 1998). In isolated OSNs, the contribution of the Cl^- current to the odorant-induced receptor current is about 80%-90% (Boccaccio and Menini, 2007; Reisert et al., 2005). The TMEM16B channel is a relatively "new" member of the transduction machinery: it was cloned from OSNs in 2009 (Stephan et al., 2009). Despite this, the contribution of the Cl^- to the receptor current has been extensively investigated since its first description in 1991 (Kleene and Gesteland, 1991). The afore mentioned unusual feature of the Cl^- current in OSNs might have evolved to render the odorant response robust against mucosal ion concentration changes (Dibattista et al., 2017; Kleene, 2008). Single OSN recordings from *Tmem16b* knock out (KO) mouse models revealed that the Cl^- contribution is substantial at various odorant concentrations (Li et al., 2018; Pietra et al., 2016) thus indicating that it serves as a non-linear amplifier of the receptor current as previously suggested (Kurahashi and Yau, 1993; Lowe and Gold, 1993).

An interesting and challenging aspect of signal transduction is that of connecting single cell response properties with olfactory behavior. How much is TMEM16B contributing to olfactory-mediated behavior? It is now clear that the Cl^- current is necessary to mediate olfactory-driven behaviors in naïve animals that require little training (i.e. finding the cookie test, track unfamiliar odor) (Neureither et al., 2017; Pietra et al., 2016; Zak et al., 2018), while after intensive training its contribution can be less relevant (Billig et al., 2011).

Editorial Decision 31 January 2023.

While isolated OSNs from *Tmem16b* KO mice lose their Cl^- current and therefore the amplification step, the summated receptor potential recorded from the surface of the intact OE, called the electro-olfactogram (EOG), showed little or no alteration (Billig et al., 2011; Neureither et al., 2017). The EOG is a field potential recording from the intact OE and it records the voltage change in the ciliary layer of the OE triggered by odorant application via a humidified air stream (Cygnar et al., 2010; Ottoson, 1955; Scott and Scott-Johnson, 2002). By using the EOG as the recording technique, the role of several transduction components have been defined. For example, *Cnga2* (a subunit of the CNG channels in OSNs) or *Adcy3* (the adenylyl cyclase producing cAMP) KO mice did not show any EOG response to most of the canonical odorant tested. These KO mice are anosmic and struggle to survive because they are unable to find food during their first postnatal days (Brunet et al., 1996; Wong et al., 2000).

Here, we decided to use the EOG technique to better understand the contribution of TMEM16B to odorant transduction in the whole epithelium. To our surprise, we found an apparent paradoxical effect. EOGs recorded from mice lacking TMEM16B channels were larger, despite the observed reduction of the receptor current by ~80%, and also faster compared to those recorded from WT. Also, the ability to adapt was altered in the KO mice. The mechanistic reason behind this phenomenon will be discussed and probably calls for a more careful reconsideration of the nature of the EOG signals. In summary, after 30 years from its first description and around 10 years since its molecular cloning, Ca^+-activated Cl^- currents in OSNs continue to surprise.

Materials and Methods

Animals and ethical approval

Mice were handled in accordance with the Italian Guidelines for the Use of Laboratory Animals and the European Union guidelines on animal research under a protocol approved by the Italian Ministry of Health. Experiments were performed on WT and *Tmem16b* KO mice of either sex. Mice had free access to water and food. For the experiments, mice were sacrificed by anaesthetizing them by CO_2 inhalation followed by decapitation. *Tmem16b* KO mice were kindly provided by Prof. Lily Jan (University of California, San Francisco, USA, Zhang *et al.*, 2017).

Immunohistochemistry

The nose with the olfactory epithelium was fixed in 4% paraformaldehyde in PBS, pH 7.4, for 4–5 h at 4°C and then decalcified in 0.5 m EDTA, pH 8, for at least 2 days, as previously described (Agostinelli et al., 2021; Gonzalez-Velandia et al., 2022). After cryoprotection in 30 % (w/v) sucrose in PBS at 4°C overnight, the tissues were frozen in optimal cutting medium compound (Bio-Optica, Milan, Italy) and stored at −80°C before sectioning with a cryostat. Coronal sections (14–16 µm thick) were cut and mounted on Superfrost Plus Adhesion Microscope Slides (ThermoFisher Scientific). Sections were air-dried for 3 h and stored at −80°C for further use. After rehydration with PBS, sections were incubated with SDS 0.5% (w/v) in PBS for antigen retrieval followed by blocking solution [5% (v/v) donkey serum and 0.3% (v/v) Triton X-100 in PBS] for 2 h and then with the polyclonal rabbit anti TMEM16B primary antibody (Novus NBP1-90739 diluted 1:1000 in the blocking solution) overnight at 4°C. Slices were then rinsed with PBS and incubated with AlexaFluor488-conjugated donkey anti rabbit secondary antibody (ThermoFisher Scientific A21206) diluted 1:250 in PBS-T (0.1% Tween 20 in PBS) for 2 h at room temperature. After washing with PBS-T, sections were treated with DAPI (0.2 µg/ml) for 30 min, washed with PBS-T, and mounted with Vectashield (VectorLaboratories, Burlingame, CA, USA). Immunofluorescence was visualized with a confocal laser scanning microscope (A1R Nikon, Tokyo, Japan). Images were acquired using NIS-Elements Nikon software at 1024 × 1024 pixels resolution and analyzed with ImageJ software (National Institute of Health, Bethesda, MD, USA).

Electro-olfactogram recordings

The experimental procedure was similar to that previously described by Zhao et al. (1998) and Franceschini et al., (2009, 2014). After the mouse was sacrificed, the head was cut sagittally and the nasal septum was carefully removed to expose the olfactory turbinates. The half heads were placed on a dissecting microscope located on a vibration-isolating table and shielded from electrical fields by a Faraday cage. The recording electrode was made from borosilicate glass (World Precision Instruments) pulled with a PP-830 puller (Narishige) to obtain a tip diameter of 10–20 µm. The tip of the pipette was filled with Ringer's solution containing 0.5% agar and the pipette was filled with Ringer's solution. Ringer's solution contained (in mM) the following: 140 NaCl, 5 KCl, 2 $CaCl_2$, 1 $MgCl_2$, 10 Hepes, pH 7.4 with NaOH. The recording electrode was mounted in a pipette holder and was carefully placed on olfactory turbinates. The ground electrode was placed in the brain of the mouse. The hydration of the epithelium was guaranteed by a constant stream of humidified and deodorized air over the turbinates. The stimulus pulse was controlled by a Picospritzer-controlled valve (Parker Hannifin). For stimulation, a 100 ms pulse of vapor phase odorant was injected at 10 psi into a continuous stream of humidified air. Vapor phase odorant as the stimulus were generated by placing an odorant solution in a 10-ml glass test tube capped with a rubber stopper. Two 20-gauge needles provided the input and output ports for the odorant-containing vapor above the solution. The odorants used, isoamyl acetate (IAA) and heptanal, were prepared every day as 5 M stocks in dimethyl sulfoxide (DMSO) and then diluted in water to reach a final concentration from 10^{-5} to 10^{-1} M. The recordings were made from 2 points on the olfactory epithelium, in the anterior region in turbinate II and in the posterior region in turbinate IV. The minimum interval between stimulations, excluding when explicitly indicated, was at least 3 minutes. Experiments were performed at room temperature. The data were collected with an Axopatch 1D amplifier controlled by Clampex 9.2 via Digidata 1322A (Axon Instruments, USA). The signals were recorded at a sampling rate of 1 kHz and low-pass filtered at 20 Hz. Analysis and figure preparation were performed using IgorPro (Wavemetrics). The kinetics of EOG responses were evaluated measuring latency, rise time and decay time. Latency was determined as the time between the start of odorant stimulation to 1% of the peak value; the rise as the time between the start of the response and the peak; the decay time (t_{75}) as the time the response takes to decrease by 75% of the peak. If not stated differently, all chemicals were purchased from Sigma.

Results

Expression of TMEM16B in the olfactory epithelium

To investigate the role of TMEM16B in olfactory transduction we used a loss-of-function approach using a KO mouse for *Tmem16b*. In these animals, the coding sequence for membrane-bound farnesylated mCherry is inserted into the *Tmem16b* locus to visualize cells expressing TMEM16B (Zhang et al., 2017). We performed immunohistochemical experiments to visualize TMEM16B in this model. As expected, in OEs from WT mice, TMEM16B was localized in the ciliary layer on the surface of the epithelium while mCherry was not expressed (Fig. 1A–C). In *Tmem16b* KO mice, no staining was detected for TMEM16B and mCherry was localized in the entire OSNs (Fig. 1D-F), as expected as mCherry *Tmem16b* KO mice were engineered to express mCherry in the entire cells that normally express TMEM16B (Zhang et al., 2017).

Odorant responses in *Tmem16b* KO OSNs

We investigated the role of TMEM16B in signal transduction by using the electro-olfactogram (EOG) technique, stimulating with two odorants individually presented at varying concentrations. We selected two different spots on the olfactory turbinates (one anterior on turbinate II and one posterior on IV, respectively) and recorded the odorant responses.

Surprisingly, we found that the odorant responses are significantly bigger in KO epithelia compared with WT both in the anterior and posterior parts of OE (Fig. 2A–D). The larger responses in KO were independent of the odorant used since we stimulated both with isoamyl acetate (IAA) or heptanal at different concentration (from 10^{-5} to 10^{-1} M). For both odorants, the difference became statistically significant at the higher concentrations that we tested. For example, in the anterior region, the average response to 10^{-1} M IAA was 13 ± 2 mV (n = 11) in the *Tmem16b* KO and 7.2 ± 1.0 mV in WT (n = 12; Fig. 2A, C). Thus, the odor response was almost two-fold larger in KO compared with WT mice.

In addition, not only the responses in the KO were larger but they were also faster. We further analyzed the kinetics of the EOG responses to IAA (Fig. 3) and found that both the rise time and the decay time (t_{75}, see Methods), were significantly faster in OEs from *Tmem16b* KO with respect to WT (Fig. 3E, F). No changes were observed in the latency (Fig. 3D). Similar results were obtained both with IAA and heptanal as stimulus.

Paired pulse adaptation responses in WT and *Tmem16b* KO mice

Odorant-induced adaptation occurs in the olfactory system to prevent the saturation of the cellular transduction machinery and can be described as the phenomena of decreasing responses either to repeated stimuli or during prolonged stimulation (Kurahashi and Menini, 1997; Reisert and Matthews, 1999).

To study the possible role of TMEM16B in OSN adaptation, we performed EOG recordings using a paired pulse protocol. We delivered two 100 ms-long IAA pulses to the anterior portion of OEs with interpulse intervals (IPI) ranging from 0.5 to 5 s (Fig. 4A, C). Since the response to the first odor pulse did not decay to baseline when the second pulse was applied, the recorded second response reflects the sum of the residual first response and the real, adapted, response to the second pulse. To obtain the net second response peak amplitude, we first fitted the decay phase of the first response with a single exponential function. Then, we subtracted the value of the fitted trace at the peak time of the second response from the second pulse peak amplitude. To quantify paired-pulse adaptation, we calculated the ratio between the peak of the second response and the first response (2nd/1st). At 10^{-4} M IAA paired pulse adaptation was similar

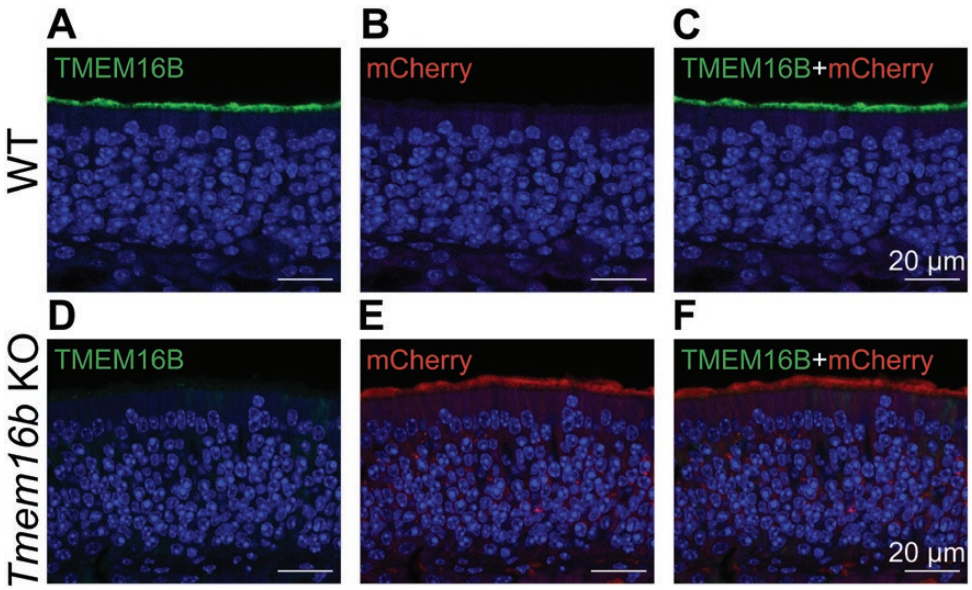

Figure 1. TMEM16B is expressed in olfactory sensory neurons. Confocal micrographs of coronal sections of the olfactory epithelium of WT (**A–C**) and *Tmem16b* KO (**D–F**). TMEM16B was expressed in the ciliary layer of WT (**A**) but not in KO mice (**D**). mCherry stains the cells of *Tmem16b* KO that normally express TMEM16B and was only detected in OSNs from KO mice (**B**, **E**). Nuclei were stained with DAPI.

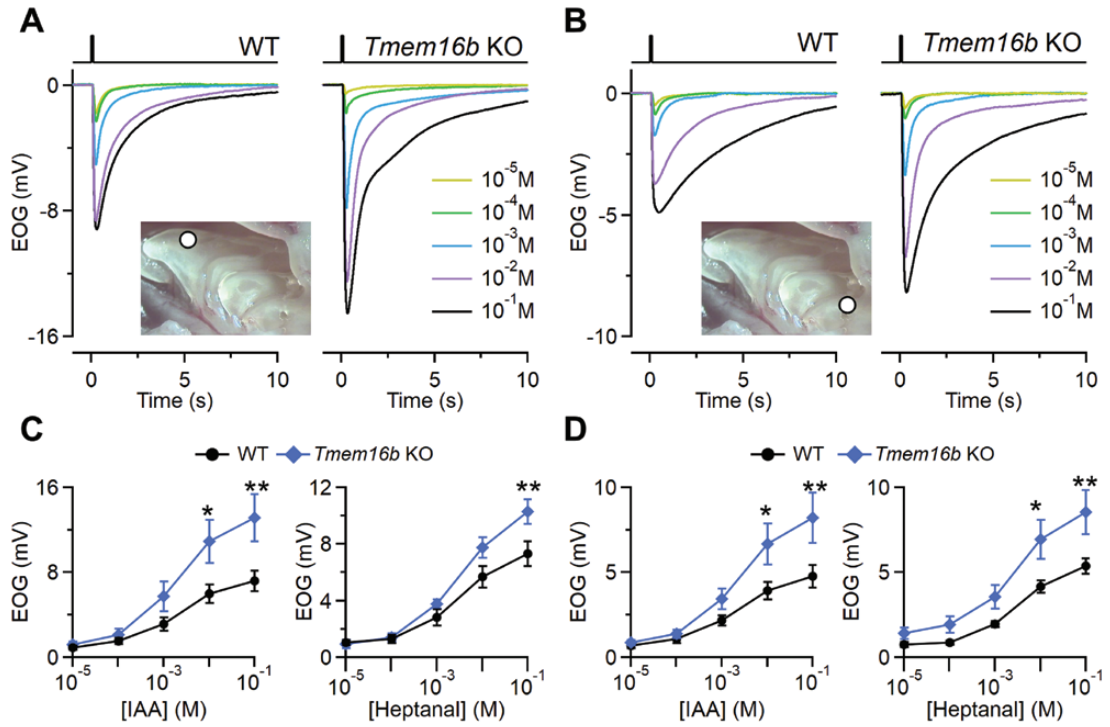

Figure 2. Odorant responses in WT and *Tmem16b* KO mice. Representative EOG recordings from WT or *Tmem16b* KO mice. The responses were evoked by 100 ms stimulation with isoamyl acetate (IAA) vapor of increasing concentrations ranging from 10^{-5} to 10^{-1} M as indicated. EOG recordings were obtained from anterior (**A**) or posterior (**B**) portions of OEs as shown in the inset. Dose–response relationships of average peak EOG amplitudes from WT or *Tmem16b* KO mice to IAA or heptanal vapor obtained from anterior (**C**) or posterior (**D**) portions of OE (n = 9–12; $^{**}P < 0.01$ $^{*}P < 0.05$ t-test with Bonferroni correction after mixed two way ANOVA). Error bars represent sem.

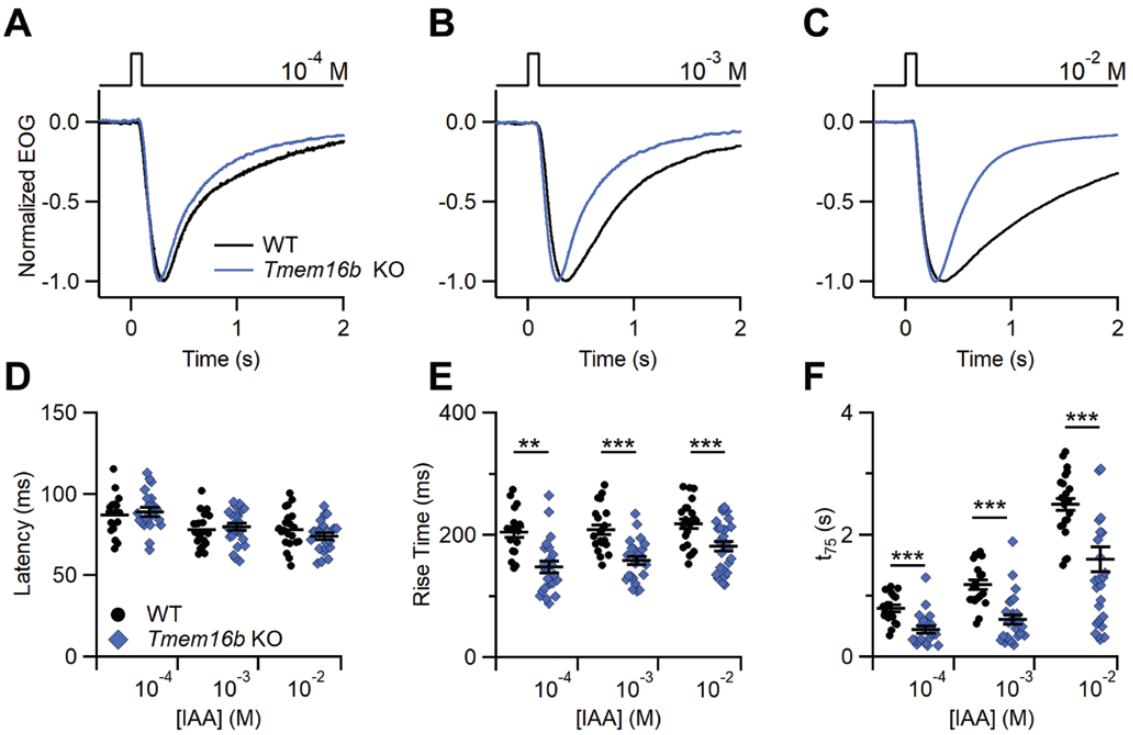

Figure 3. Kinetics of the odorant response in WT and *Tmem16b* KO mice. (**A–C**) Representative normalized EOG recordings from WT or *Tmem16b* KO mice. The responses were evoked by 100 ms stimulation of vapors of the indicated IAA solution concentration. Scatter dot plot with average ± sem showing the values of latency (**D**), rise time (**E**) and decay time (t_{75}) (**F**) in WT or *Tmem16b* KO mice at each odorant concentration (n = 17–21; $^{**}P < 0.01$ $^{***}P < 0.01$ Student's t test).

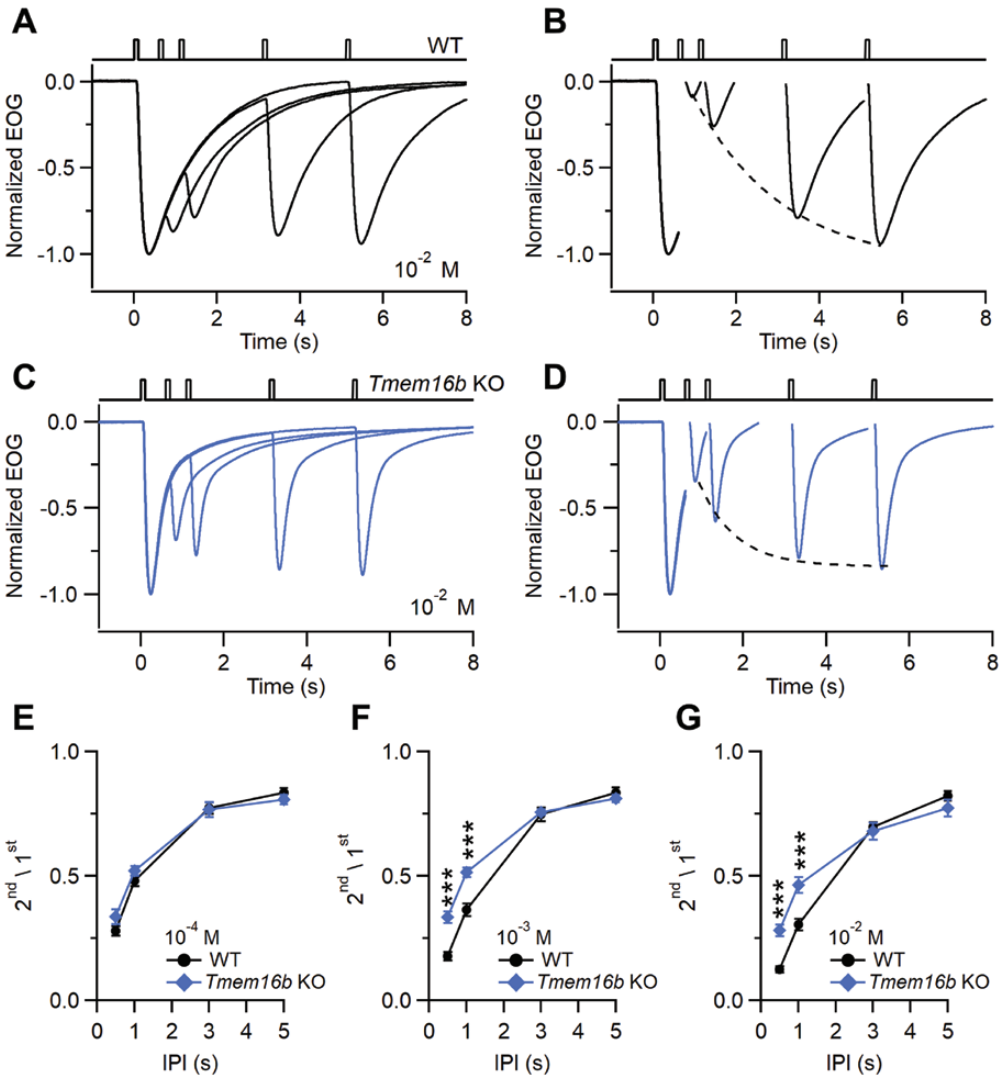

Figure 4. Paired pulse odorant responses in WT and *Tmem16b* KO mice. Representative normalized EOG double pulse responses from WT (**A**) and *Tmem16b* KO mice (**C**). OEs were stimulated with 100 ms-long pulses with different interpulse intervals (IPI 0.5, 1, 3, 5 s) with IAA at 10^{-2} M concentration. (**B, D**) Net responses to each stimulus for the recordings are shown in (**A–C**). Dotted line represents the mono-exponential fit obtained with the peak responses to the second odor pulses. (**E–G**) Ratio of the second stimulus to the first ± sem at the indicated odorant concentration plotted versus the IPI (n = 8–10; ***$P < 0.001$ t-test with Bonferroni correction after mixed two-way ANOVA).

in *Tmem16b* KO and WT mice (Fig. 4E). At high odorant concentrations (10^{-3} M and 10^{-2} M IAA), we found that responses from *Tmem16b* KO recovered faster from adaptation than WT mice. At 10^{-3} M IAA, the ratio 2nd/1st for IPI 0.5 s was 0.17 ± 0.02 for WT (n = 9) and 0.33 ± 0.02 for *Tmem16b* KO (n = 10), while for IPI of 1 s, the ratio 2nd/1st was 0.51 ± 0.02 for WT (n = 9) and 0.38 ± 0.02 for KO (n = 10; Fig. 4F). Similar differences were found at 10^{-2} M IAA (Fig. 4G). The striking differences in paired-pulse stimulations at low odorant concentrations indicate that in *Tmem16b* KO adaptation to the second odorant stimulus was reduced with respect to WT at the shorter IPI up to 1 s and it was dependent on the odorant concentration. The results shown in Fig. 4 were recorded from turbinate II and similar results were obtained from turbinate IV of the OE. Also, the faster recovery from adaptation observed in the *Tmem16b* KO compared with WT mice was odorant independent since similar results were obtained using heptanal as stimulus.

Discussion

The very first step in odor perception is the activation of the peripheral odorant transduction cascade that gives rise to the transduction current characterized by response amplitude and kinetics that must be tuned to the always-changing odorant landscape (Boccaccio et al., 2021; Genovese et al., 2021; Kleene, 2008). TMEM16B is the main Ca^{+}-activated Cl^{-} channel playing a role in odorant transduction. Using single cell electrophysiology, it was shown that the Ca^{+}-activated Cl^{-} currents were entirely absent in OSNs from *Tmem16b* KO mice (Billig et al., 2011; Li et al., 2018, 2022; Pietra et al., 2016; Ponissery Saidu et al., 2013; Stephan et al., 2009). Several laboratories tried to clarify further the role of this channel (Billig et al., 2011; Li et al., 2018; Neureither et al., 2017; Pietra et al., 2016) and its current that normally constitute up to 90% of the receptor current in rodents (Boccaccio and Menini, 2007; Kurahashi and Yau, 1993; Lowe and Gold, 1993; Reisert et al., 2005).

Here we showed that TMEM16B limits the amplitude and prolongs the odorant-evoked field potentials. Our data introduce what seems to be a paradoxical effect: while amplifying the transduction currents recorded in single cells (Boccaccio and Menini, 2007; Lowe and Gold, 1993; Reisert et al., 2005), TMEM16B apparently reduces the summated generator potentials.

Also, we investigated odorant-induced adaptation by measuring EOGs in response to repeated odorant stimuli with various interpulse intervals. Adaptation was present both in olfactory epithelia from WT and *Tmem16b* KO mice but the absence of TMEM16B induced a faster recovery from adaptation only at high odorant concentrations and short interpulse intervals, indicating that TMEM16B has a limited role in paired pulse adaptation when measured with EOG recordings.

Our paper is not the first to measure EOG responses from OE of *Tmem16b* KO mouse models. Two previous studies used EOG recordings to understand the role of TMEM16B in olfactory transduction and reported contrasting results (Billig et al., 2011; Neureither et al., 2017). Billig et al. (2011) used EOG recordings both in the fluid phase, where they measured a response reduction in *Tmem16b* KO and EOG recordings in the air phase, where they did not observe any substantial changes in the odorant-induced responses. As they also did not find any apparent behavioral deficits, they considered TMEM16B and its currents dispensable for normal olfaction. Later, Neureither et al. (2017) showed that the integral of the air phase EOG responses were significantly smaller in KO compared with WT at low concentrations of the food-related attractive odorant syringol, while no differences were found at higher concentrations. The authors did not mention whether there was a decrease in EOG response peak amplitudes.

Our results introduce a third scenario where EOG responses from KO are larger and faster compared to the WT mice. The reasons for these discrepancies with the afore mentioned published results are not clear. For example, technical differences in air and odorant application (flow rate, pressure, humidity) could explain the contrasting results (Scott et al., 1996, 1996). Another possible difference could be the different odorants used as stimuli. It is also worth noting that in Billig et al, (2011) the magnitude of the EOG air phase responses were quite small, less than 0.5 mV, probably dampening the possibility of detection of small but significant differences; while in Neureither et al. (2017), the authors themselves mentioned that their responses were quite variable and for this reason they decided to use the integral of the response as the measured parameter. Our EOG experiments instead showed consistently larger peak responses and although the experimenter was blinded to the genotype, could quickly distinguish between WT and KO because at higher concentrations the responses were clearly larger and faster. In summary, in *Tmem16b* KO compared to WT mice, the EOG responses have been reported to be either one of the following: unchanged, but very small (Billig et al., 2011), smaller integrated responses, that would be compatible with faster responses (Neureither et al., 2017), or larger and faster (this paper).

It is difficult to find a common denominator that could satisfactorily explain these different results but we believe that a first conclusion that could be drawn is that EOG potentials are changed in the KO mice. In addition, Neureither et al. (2017); Zak et al. (2018) and our previous report (Pietra et al., 2016) showed that *Tmem16b* KO mice failed to perform naïve olfactory tasks that did not required a learning phase.

Since single cell recordings showed drastic reductions in the transduction current in KO mice (Billig et al., 2011; Li et al., 2018; Pietra et al., 2016), one could expect that also the EOG amplitude could be decreased, but these two recording methods might not necessarily match in every aspect. For example, in KO mice for the cilia- and flagella-associated protein 69 (*Cfap69)*, the transduction currents measured from isolated single OSNs were unaltered in their maximal responses, while EOG amplitude were reduced at higher concentrations of amyl acetate (Talaga et al., 2017). Furthermore, using single cell suction recordings, the $Na^+/K^+/2Cl^-$ transporter 1 (NKCC1) has been shown to be necessary and sufficient for Cl^- accumulation in OSNs cilia (Hengl et al., 2010; Kaneko et al., 2004; Reisert et al., 2005). However, EOG recordings have shown contrasting results (Haering et al., 2015; Nickell et al., 2006, 2007), indicating that more than one transporter might be involved in Cl^- accumulation (Nickell et al., 2006, 2007). Of note, in this case Cl^- homeostasis was altered, not the Ca^{2+}-activated Cl^- channel.

One could ask: is the EOG really measuring only the transduction events? EOGs have been extensively shown to be generated by OSNs (Ottoson, 1955; Scott and Scott-Johnson, 2002) and reflecting transduction processes (Belluscio et al., 1998; Brunet et al., 1996; Wong et al., 2000). EOGs are also the result of odorant stimulation with a contribution from other events and/or other cells that are excited indirectly as a consequence of OSN response (Daiber et al., 2013; Lu et al., 2008). In order to contribute to EOGs, those other signals must be slow events at the timescale of the EOG that fall in the time windows of the recorded response; i.e. fast Na^+ spikes are unlikely contributors to the normal EOG signals (Genovese et al., 2016). When EOG recordings were performed from mice with mature OSNs expressing channelrhodopsin in the whole cellular membrane except in the ciliary membrane, the light-induced potentials were faster and had smaller amplitudes (Genovese et al., 2016) compared to the canonical EOG recorded odorant responses. The answer to the above question is then that transduction events have a predominant role in the EOG responses.

What do EOG results tell us about the physiological role of TMEM16B? We proposed that the role of the Ca^+-activated Cl^- currents is to clamp the membrane potential during an odorant stimulation thus keeping sodium channels inactivated reducing the length and the number of action potentials (Pietra et al., 2016). In addition, TMEM16B is also contributing to the spontaneous firing of the OSNs induced by basal OR activity (Dibattista and Reisert, 2016; Reisert, 2010) Therefore, the lack of TMEM16B could cause a reduction of the basal Cl^- conductance decreasing the ciliary conductance and increasing the net odorant-evoked depolarization. Moreover, the Cl^- intraciliary and mucus concentrations may set the reversal potential for a Cl^- current to be more negative than that for the CNG-mediated currents (that have a reversal close to 0 mV). In these conditions, Ca^+-activated Cl^- currents would shunt the CNG channel depolarization (hence reduce the maximal response generated by the CNG channel alone). The altered EOG responses would then indicate that the lack of TMEM16B confounds the entire peripheral information processing, thus altering the signals arriving to the olfactory bulb (Zak et al., 2018).

Single cell recordings, although powerful to understand transduction do not inform on the population-wise events within the entirety of the olfactory epithelium. EOGs, instead, by recording an ensemble of odorant responses from OSNs expressing both the same and different ORs, may represent the very first population-wise information processing in the entire olfactory system. In conclusion, TMEM16B might limit membrane depolarization, control spike train duration and the amplitude and kinetics of the OSN generator potential recorded by the EOG.

Authors Contribution

G.G. performed electro-olfactogram, immunohistochemistry and confocal microscopy, G.G. and S.P. analyzed the data, S.P., A.M., M.D., and J.R. designed experiments, S.P., A.M., M.D., and J.R. wrote the manuscript with comments from all the other authors.

Conflict of interest statement

The authors have no conflicts of interest to declare.

Funding

This work was supported by funding from the National Institutes of Health (NIH) grant R01DC016647 and R01DC009613 to Johannes Reisert.

Data Availability

The data underlying this article will be shared on reasonable request to the corresponding authors.

References

Agostinelli E, Gonzalez-Velandia KY, Hernandez-Clavijo A, Kumar Maurya D, Xerxa E, Lewin GR, Dibattista M, Menini A, Pifferi S. A Role for STOML3 in Olfactory Sensory Transduction. *ENeuro*. 2021;8:ENEURO.0565ENEURO.0565-20.2021–ENEURO.0565ENEURO.0565-20.2021.

Belluscio L, Gold GH, Nemes A, Axel R. Mice deficient in G(olf) are anosmic. *Neuron*. 1998;20:69–81.

Billig GM, Pál B, Fidzinski P, Jentsch TJ. Ca2+-activated Cl– currents are dispensable for olfaction. *Nat Neurosci*. 2011;14:763–769.

Boccaccio A, Menini A. Temporal development of cyclic nucleotide-gated and Ca2+ -activated Cl- currents in isolated mouse olfactory sensory neurons. *J Neurophysiol*. 2007;98:153–160.

Boccaccio, A, Menini, A., Pifferi, S. The cyclic AMP signaling pathway in the rodent main olfactory system. *Cell Tissue Res*. 2021;383:429–443.

Bradley J, Reisert J, Frings S. Regulation of cyclic nucleotide-gated channels. *Curr Opin Neurobiol*. 2005;15:343–349.

Brunet LJ, Gold GH, Ngai J. General anosmia caused by a targeted disruption of the mouse olfactory cyclic nucleotide-gated cation channel. *Neuron*. 1996;17:681–693.

Cygnar KD, Stephan AB, Zhao H. Analyzing responses of mouse olfactory sensory neurons using the air-phase electroolfactogram recording. *J Vis Exp JoVE*. 2010;1850.

Daiber P, Genovese F, Schriever VA, Hummel T, Möhrlen F, Frings S. Neuropeptide receptors provide a signalling pathway for trigeminal modulation of olfactory transduction. *Eur J Neurosci*. 2013;37:572–582.

Dibattista M, Pifferi S, Boccaccio A, Menini A, Reisert J. The long tale of the calcium activated Cl- channels in olfactory transduction. *Channels Austin Tex*. 2017;11:399–414.

Dibattista M, Reisert J. The odorant receptor-dependent role of olfactory marker protein in olfactory receptor neurons. *J Neurosci Off J Soc Neurosci*. 2016;36:2995–3006.

Franceschini V, Bettini S, Pifferi S, Menini A, Siciliano G, Ognio E, Brini AT, Di Oto E, Revoltella RP. Transplanted human adipose tissue-derived stem cells engraft and induce regeneration in mice olfactory neuroepithelium in response to dichlobenil subministration. *Chem Senses*. 2014;39:617–629.

Franceschini V, Bettini S, Pifferi S, Rosellini A, Menini A, Saccardi R, Ognio E, Jeffery R, Poulsom R, Revoltella RP. Human cord blood CD133+ stem cells transplanted to nod-scid mice provide conditions for regeneration of olfactory neuroepithelium after permanent damage induced by dichlobenil. *Stem Cells Dayt Ohio*. 2009;27:825–835.

Genovese F, Reisert J, Kefalov VJ. Sensory transduction in photoreceptors and olfactory sensory neurons: common features and distinct characteristics. *Front Cell Neurosci*. 2021;15:761416.

Genovese F, Thews M, Möhrlen F, Frings S. Properties of an optogenetic model for olfactory stimulation. *J Physiol*. 2016;594:3501–3516.

Gonzalez-Velandia KY, Hernandez-Clavijo A, Menini A, Dibattista M, Pifferi S. Expression pattern of Stomatin-domain proteins in the peripheral olfactory system. *Sci Rep*. 2022;12:11447.

Haering C, Kanageswaran N, Bouvain P, Scholz P, Altmüller J, Becker C, Gisselmann G, Wäring-Bischof J, Hatt H. Ion transporter NKCC1, modulator of neurogenesis in murine olfactory neurons. *J Biol Chem*. 2015;290:9767–9779.

Hengl T, Kaneko H, Dauner K, Vocke K, Frings S, Möhrlen F. Molecular components of signal amplification in olfactory sensory cilia. *Proc Natl Acad Sci USA*. 2010;107:6052–6057.

Kaneko H, Putzier I, Frings S, Kaupp UB, Gensch T. Chloride accumulation in mammalian olfactory sensory neurons. *J Neurosci Off J Soc Neurosci*. 2004;24:7931–7938.

Kleene SJ. The electrochemical basis of odor transduction in vertebrate olfactory cilia. *Chem Senses*. 2008;33:839–859.

Kleene SJ, Gesteland RC. Calcium-activated chloride conductance in frog olfactory cilia. *J Neurosci Off J Soc Neurosci*. 1991;11:3624–3629.

Kurahashi T, Menini A. Mechanism of odorant adaptation in the olfactory receptor cell. *Nature*. 1997;385:725–729.

Kurahashi T, Yau KW. Co-existence of cationic and chloride components in odorant-induced current of vertebrate olfactory receptor cells. *Nature*. 1993;363:71–74.

Li R-C, Lin C-C, Ren X, Wu JS, Molday LL, Molday RS, Yau K-W. Ca2+-activated Cl current predominates in threshold response of mouse olfactory receptor neurons. *Proc Natl Acad Sci USA*. 2018;115:5570–5575.

Li R-C, Molday LL, Lin C-C, Ren X, Fleischmann A, Molday RS, Yau K-W. Low signaling efficiency from receptor to effector in olfactory transduction: a quantified ligand-triggered GPCR pathway. *Proc Natl Acad Sci USA*. 2022;119:e2121225119.

Lowe G, Gold GH. Nonlinear amplification by calcium-dependent chloride channels in olfactory receptor cells. *Nature*. 1993;366:283–286.

Lu DC, Zhang H, Zador Z, Verkman AS. Impaired olfaction in mice lacking aquaporin-4 water channels. *FASEB J Off Publ Fed Am Soc Exp Biol*. 2008;22:3216–3223.

Mombaerts P. Genes and ligands for odorant, vomeronasal and taste receptors. *Nat Rev Neurosci*. 2004;5:263–278.

Nakamura T, Gold GH. A cyclic nucleotide-gated conductance in olfactory receptor cilia. *Nature*. 1987;325:442–444.

Neureither F, Stowasser N, Frings S, Möhrlen F. Tracking of unfamiliar odors is facilitated by signal amplification through anoctamin 2 chloride channels in mouse olfactory receptor neurons. *Physiol Rep*. 2017;5:e13373.

Nickell WT, Kleene NK, Gesteland RC, Kleene SJ. Neuronal chloride accumulation in olfactory epithelium of mice lacking NKCC1. *J Neurophysiol*. 2006;95:2003–2006.

Nickell WT, Kleene NK, Kleene SJ. Mechanisms of neuronal chloride accumulation in intact mouse olfactory epithelium. *J Physiol*. 2007;583:1005–1020.

Ottoson D. Analysis of the electrical activity of the olfactory epithelium. *Acta Physiol Scand Suppl*. 1955;35:1–83.

Pietra G, Dibattista M, Menini A, Reisert J, Boccaccio A. The Ca2+-activated Cl- channel TMEM16B regulates action potential firing and axonal targeting in olfactory sensory neurons. *J Gen Physiol*. 2016;148:293–311.

Pifferi, S, Cenedese, V., Menini, A. Anoctamin 2/TMEM16B: a calcium-activated chloride channel in olfactory transduction. *Exp Physiol*. 2012;97:193–199.

Ponissery Saidu S, Stephan AB, Talaga AK, Zhao H, Reisert J. Channel properties of the splicing isoforms of the olfactory calcium-activated chloride channel Anoctamin 2. *J Gen Physiol*. 2013;141:691–703.

Reisert J. Origin of basal activity in mammalian olfactory receptor neurons. *J Gen Physiol*. 2010;136:529–540.

Reisert J and Matthews HR. Adaptation of the odour-induced response in frog olfactory receptor cells. *J Physiol*. 1999;519:801–813.

Reisert J, Lai J, Yau K-W, Bradley J. Mechanism of the excitatory Cl- response in mouse olfactory receptor neurons. *Neuron*. 2005;45:553–561.

Reuter D, Zierold K, Schröder WH, Frings S. A depolarizing chloride current contributes to chemoelectrical transduction in olfactory sensory neurons in situ. *J Neurosci Off J Soc Neurosci*. 1998;18:6623–6630.

Scott JW, Davis LM, Shannon D, Kaplan C. Relation of chemical structure to spatial distribution of sensory responses in rat olfactory epithelium. *J Neurophysiol*. 1996;75:2036–2049.

Scott JW, Scott-Johnson PE. The electroolfactogram: a review of its history and uses. *Microsc Res Tech*. 2002;58:152–160.

Stephan AB, Shum EY, Hirsh S, Cygnar KD, Reisert J, Zhao H. ANO2 is the cilial calcium-activated chloride channel that may mediate olfactory amplification. *Proc Natl Acad Sci USA*. 2009;106:11776–11781.

Talaga AK, Dong FN, Reisert J, Zhao H. Cilia- and Flagella-Associated Protein 69 Regulates Olfactory Transduction Kinetics in Mice. *J Neurosci Off J Soc Neurosci*. 2017;37:5699–5710.

Tirindelli R, Dibattista M, Pifferi S, Menini A. From pheromones to behavior. *Physiol Rev*. 2009;89:921–956.

Torre V, Ashmore JF, Lamb TD, Menini A. Transduction and adaptation in sensory receptor cells. *J Neurosci Off J Soc Neurosci*. 1995;15:7757–7768.

Wong ST, Trinh K, Hacker B, Chan GC, Lowe G, Gaggar A, Xia Z, Gold GH, Storm DR. Disruption of the type III adenylyl cyclase gene leads to peripheral and behavioral anosmia in transgenic mice. *Neuron*. 2000;27:487–497.

Zak JD, Grimaud J, Li R-C, Lin C-C, Murthy VN. Calcium-activated chloride channels clamp odor-evoked spike activity in olfactory receptor neurons. *Sci Rep*. 2018;8:10600.

Zhao H, Ivic L, Otaki JM, Hashimoto M, Mikoshiba K, Firestein S. Functional expression of a mammalian odorant receptor. *Science*. 1998;279:237–242.

Zhang Y, Zhang Z, Xiao S, Tien J, Le S, Le T, Jan LY, Yang H. Inferior Olivary TMEM16B Mediates Cerebellar Motor Learning. *Neuron*. 2017;95:1103–1111.e4.